STEEL STRUCTURES
www.ijoss.org
Steel Structures 8 (2008) 119-133

Effect of Stiffener Details on Behavior of CFT Column-to-Beam Connections

Young-Ju Kim[1], Kyung-Jae Shin[2,*] and Wha-Jung Kim[3]

[1]*Research professor, Dept. of Civil, Environmental and Architectural Engineering, Korea University, 5 Anam-dong, Seongbuk-gu, Seoul 136-701, Korea*
[2]*Professor, Dept. of Architectural Engineering, Kyungpook National University, 1370 Sankyuk-dong, Buk-gu, Daegu 702-701, Korea*
[3]*Professor, Dept. of Architectural Engineering, Kyungpook National University, 1370 Sankyuk-dong, Buk-gu, Daegu 702-701, Korea*

Abstract

The objective of this research is to understand stress-transfer mechanism of concrete-filled tube (CFT) column-to-beam connections with external T-stiffener by using a nonlinear finite element analysis and to offer basic data for the design of T-stiffener connection. Firstly, the same shapes of the full-scale test specimens were modeled for the finite element analysis to delineate the problems of previous test results, The models of analysis with different T-stiffener are grouped into T-stiffener (TS series), T-stiffener with a dog bone (TSD series), i.e., reduced beam section (RBS cutout), and T-stiffener with holes in horizontal element (TSH series). Results of the nonlinear finite element analysis were compared with the test results. Secondly, a parametric study was conducted to investigate an alternative plan that decreases the concentration of stress in the connection. The main parameters were the types of horizontal elements, the ratio of horizontal and vertical element strength to beam strength, presence of RBS cutout, and size of holes. Several stress and strain indices were used understand the stress-transfer mechanism of the connection with various T-stiffeners parameters. The basic design ideas are recommended based on various performance indices in relation to the connection details.

Keywords: Connection, T-stiffener, Concrete-filled tube, Stress-transfer mechanism, Plastic strain

1. Introduction

The steel moment-resisting frame, in general, is considered to be a structure of excellent ductility and is widely used in high-rise buildings. Recently, CFT has drawn a widespread interest as column members of steel structures. Compared to conventional steel or other composite columns, CFT columns possess many advantages such as confinement and convenient formwork for the concrete core provided by the steel tube, improved stability and stiffness of the steel tube owing to the concrete filled into the column, and lower construction cost (Ricles *et al*., 1996; Morino *et al.*, 2005). While many advantages exist, the use of CFT column in building construction has been limited due to the lack of construction experience and the complexity of connection detailing, and these components have yet to be investigated to bring about their full potential with respect to this application. The connection details using rectangular tube column are complicated because a tube column has a closed shape. Connection between beam and column is one of the main areas in which potential cost saving can be achieved.

Due to the requirement for its practical application, numerous research works have recently been carried out in the research area related to the connection between beam and column as follows: investigation of the performance of CFT column-to-H beam connections with vertical stiffener plates (Matsuda *et al*., 2000; Kimura *et al.*, 2005), investigation of the connection details and shear strength in the panel zone of CFT through beam connections (Fukumoto *et al.*, 2000; Cheng *et al*., 2003; Azizinamini, 2005), the US-Japan cooperative earthquake research program (Fujimoto *et al*., 1997; Azizinamini *et al*., 2004; Ricles *et al*., 2004; Nishiyama *et al*., 2004), and investigation of the seismic performance of bidirectional bolted beam-to-column connections for CFTs (Wu *et al*., 2007).

Regarding the beam-to-column connections with CFTs, the most convenient connection is to attach the steel beam through the external diaphragm plate. The external

This manuscript for this paper was submitted for review and possible publication on June 4, 2008; approved on June 28, 2008.

*Corresponding author
Tel: +82-53-950-5591; Fax: +82-53-950-6590
E-mail: shin@knu.ac.kr

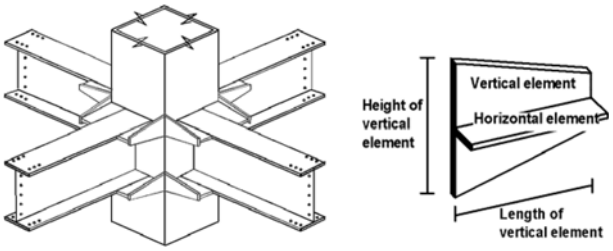

Figure 1. Schematic diagram of beam-to-column connection using T-stiffeners.

diaphragm is more efficient from both manufacturing and casting concrete compared to internal or through diaphragms. Therefore recent investigations have focused on the development of practical details for external diaphragm connections to CFTs. The connection type studied in this paper is T-stiffeners attached to the beam flanges, as shown in Fig. 1. T-stiffener consists of a horizontal and a vertical element. Fig. 2 shows the construction and setup of the connection with T-stiffeners at a construction site. After the columns, which were shop-welded with T-stiffeners and beam stubs, are erected in the field, the beam can be hoisted in place and bolted as illustrated in Fig. 2. Shanmugam and Ting (1995) investigated such a work, examining the effect of externally stiffened connections on behavior of box-column to I-beam connections both experimentally and analytically. T-stiffeners connections for CFT building structures were proposed by Shin *et al.* (1998). In their study, a test for T-stiffener connections with penetrated elements was performed, and it was found out that the T-stiffener connection has a good earthquake-resistance behavior and also that T-stiffeners played a more important role in connection performance than penetrated-elements. Kang *et al.* (2001) conducted a small-scale T-stiffener connections test, resulting in that brittle fractures occurred at the corner of the cold-formed column wall welded to the T-stiffeners. Shin *et al.* (2004) conducted full-scale connection tests using built-up CFT columns. Test results indicated that specimens exhibited good inelastic behavior but some of the connections failed in a brittle manner. It was reasoned that the initial crack developed at the tip of the horizontal element due to the stress concentration caused by the abrupt change in beam flange geometry. Thus, improved T-stiffener connection details were proposed and tested by Shin *et al.* (2008) to achieve more reliable inelastic behavior of the T-stiffener connections. In addition, a simple design procedure was also suggested for the T-stiffener connections. Test results showed that T-stiffener connections with tapered horizontal elements, with a RBS or with horizontal element holes, was very effective in reducing the propensity for cracking at the horizontal element tip by pushing both plastic hinging and local buckling away from the T-stiffener end.

The purpose of this study is to investigate the factors that can reduce the stress concentration at the connection of horizontal stiffeners and beam flange and to provide basic data required for the design of the connection by delineating the stress-transfer mechanism of the connection with various T-stiffeners parameters. Based on the results of the previous research (Shin *et al.*, 2008), a parametric study was carried out using a nonlinear finite element analysis program (ABAQUS, 2002), which was conducted to identify the stress-transfer mechanism based on the previous full-scale tests. The influence of the type of horizontal elements, the ratio of horizontal element strength to beam strength, and the presence of RBS cutout and holes on seismic performance of beam-to-column connection, is reported in this paper.

2. Summary of Previous Test Results

As mentioned in previous section, this study was conducted to delineate the stress-transfer mechanism that could not be explained by previous full-scale tests (Shin *et al.*, 2008). Improved T-stiffener connections have been proposed and exhibited good seismic performance. A result of the previous test is summarized below.

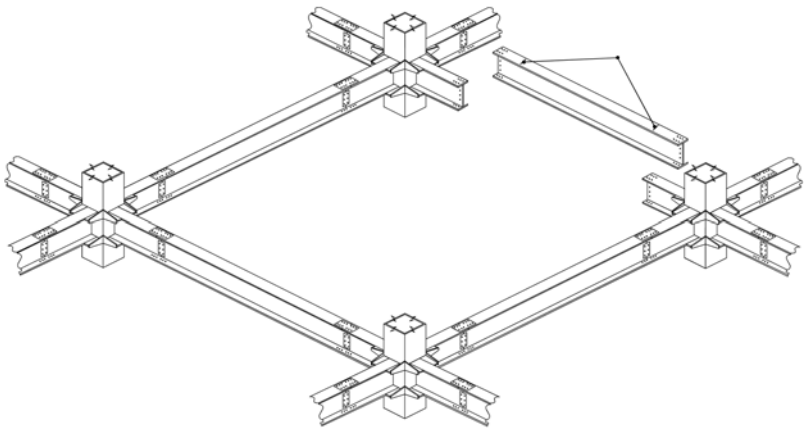

Figure 2. Construction and setup of T-stiffener connection at a construction site.

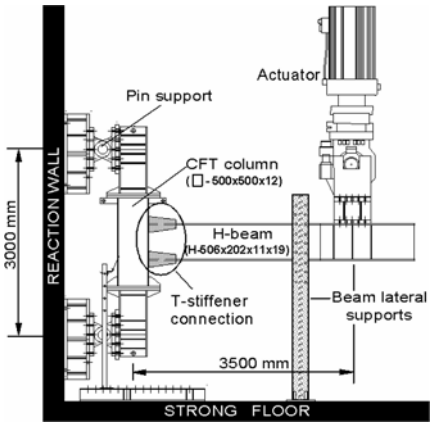

Figure 3. Test setup.

The test specimens were prepared using a built-up square tube column −500×500×12 (dimension in mm for column depth, width, and thickness of column, respectively) and wide flange beam H −512×201×11×19 (dimension in mm for beam depth, width, web thickness and flange thickness), as shown in Fig. 3. All of the seven full-scaled specimens were designed and manufactured as illustrated in Fig.4. The specimens listed in Table 1 were divided into three series, TS series, TSD series and TSH series. In the specimen designation, the following abbreviations are hereafter used: TS = T-stiffener, D = dog bone and H = hole.

In Fig.4 (a), TS series include specimens of TS100, TS120 and TS140. TS100 is a typical T-stiffener connection. In the TS series, the inner length is increased while the outer one of horizontal element is unchanged, resulting in an increase of the ratio of the horizontal element strength (H) to the beam flange strength (B). In TS series, as the ratio of the horizontal element strength to the beam flange strength (H/B) increases, the inner length only is increased while the outer one of horizontal element is unchanged. The inner length of TS120 and TS140 are 1.2 and 1.4 times, respectively, larger than that of TS100, transitioning from rectangular section to tapered section in order to reduce the stress concentration at the T-stiffener end. Test results showed that the tapered shape of the horizontal element had a significant effect on the local strain demand at the tip of horizontal element. TSD series consisted of the specimens of TSD100 and TSD120 (Fig. 4(b)). In this case, T-stiffener is used to supplement the reduced beam section (RBS) to further limit the stress in beam flange welds for the connections. It was experimentally shown that a combined strategy of using T-stiffener reinforcement plus RBS was very

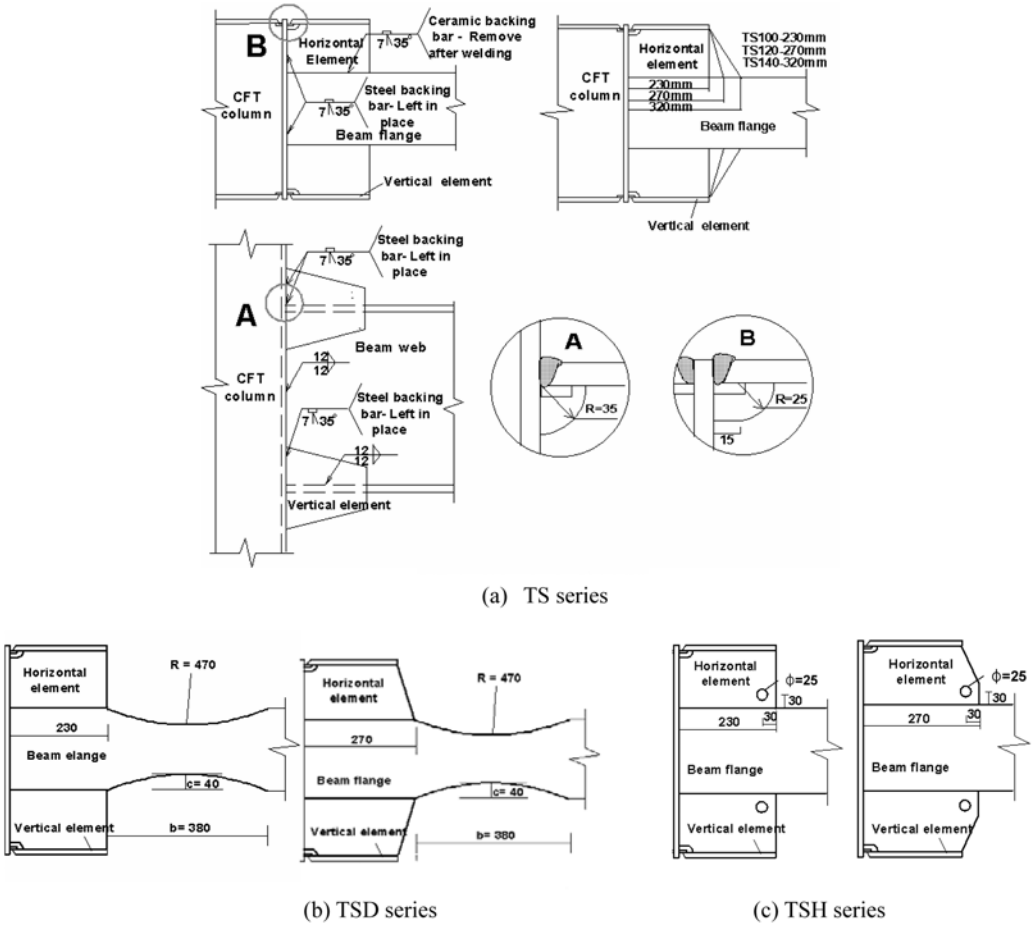

(a) TS series

(b) TSD series (c) TSH series

Figure 4. Details of connection subassemblies.

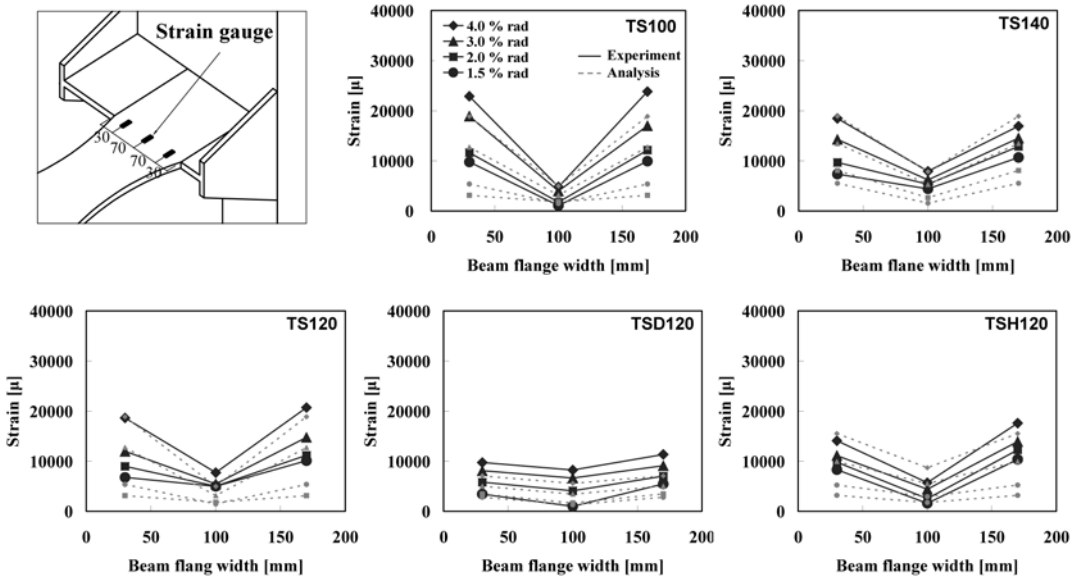

Figure 5. Variation of tensile strain across beam flange for various displacement levels.

effective in reducing the propensity for cracking at the horizontal element tip by pushing both the plastic hinging and local buckling away from the T-stiffener end. TSH series is T-stiffener connections supplemented with a hole of 25 mm size near the tip of horizontal element (Fig. 4(c)). TSH series specimens were also effective in preventing the concentration of stress.

Despite relatively good seismic performance of T-stiffener connections, detrimental effects on the connection were observed. As shown in Fig. 10(a), TS100 resulted in fractures of the beam flange. The crack in the beam flange was initiated at the tip of the horizontal element due to the concentration of stress caused by abrupt geometrical changes at the tip of the horizontal elements. This initial crack was soon followed by a sudden fracture of the entire beam flange. Fig. 5 shows the variation of stress across beam flange for each specimen at various displacement levels. The strain level of TS140 was smaller than that of TS100, and that of TSD120 as well as that of TSH120 was also smaller than the strain level of TS120. This result revealed that the tapered shape of gradual change from beam flange to horizontal element and RBS cutout in the beam brought about a considerable reduction in the concentration of strain at the T-stiffener end. TS120 and TSD100 failed by premature factures at the vertical element welds (Fig. 10(b) & 10(d)). Considering the strain-hardening factor of beam material, the strength ratio of 1.0 may not be able to ensure an adequate margin of safety to transfer the force sufficiently from vertical element to column wall. In the previous study (Shin *et al*., 2008), it was tentatively suggested that the strain-hardening factor of 1.2 was to be adopted as the strength ratio between vertical and horizontal element in order to develop the good ductility for T-stiffener connections. In case of TSH series, the effect of holes drilled in the horizontal elements has yet to become clear since the test was based on a very limited experimental study. Therefore, further studies are needed to clarify the causes of the brittle fracture of beam flanges and vertical elements welds and to investigate the effect of the holes drilled in the horizontal element.

3. Finite Element Model Analysis

3.1. Finite element model

Finite element model (FEM) analysis was carried out to identify the stress transfer-transfer mechanism of various T-stiffener connections. The characteristics of the analytical subassemblies were derived from the geometry of previous test results (shin *et al*., 2008), as shown in Fig. 4. Computer models of the test assembly were developed using a general-purpose nonlinear finite element analysis (FEA) program, ABAQUS. The three-dimensional finite element models are shown in Fig. 6. The finite element model used in this study was an integration element reduced to eight-node bricks. This analytical model was classified into (1) an overall model designed to analyze the general behavior and (2) a half model designed for a parametric study considering the analysis time and convergence.

Nonlinearity of materials is accounted for in monotonic analyses through an isotropic classical plasticity model based on the Von Mises yield criterion and the plastic flow of materials. The nominal stress-strain curves as reported in various experiments are adjusted to establish true stress-plastic strain curves for KS SS400 steels (nominal stress of 235 MPa), as shown in Fig. 7. Isotropic hardening is assumed for monotonic analysis, whereas kinematic hardening is assumed for cyclic hardening. In previous test (shin *et al*., 2008), gas metal arc welding (GMAW) with CO2 shielding was used to fabricated the welded joints of test specimens. Welding electrodes

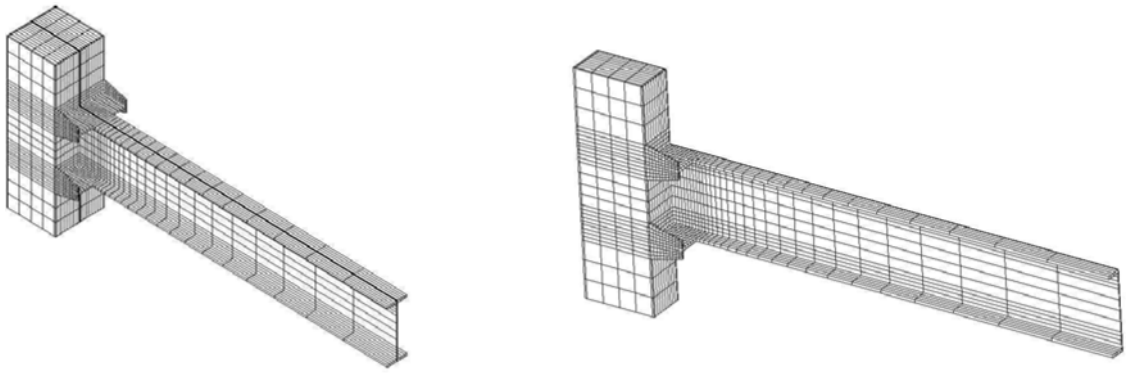

(a) Overall model (b) 1/2-scaled model

Figure 6. Details of finite element models.

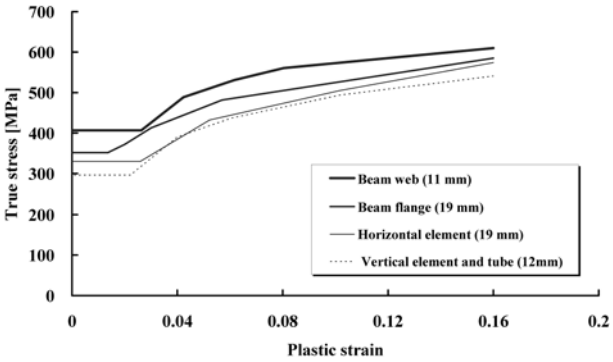

Figure 7. True stress-plastic strain curves.

designated as ER70S-3 with specified minimum CVN toughness of 80 J at −20°C were used. However, the groove welds joining the beam to column flange, the horizontal element to the beam flange and the column flange, and the vertical element to column flange were not modeled explicitly, because this study did not focused on the potential for fracture propagation of welding electrodes. In this study, the surfaces of contact were used in consideration of the filling effect of the concrete. The mechanical interaction of an interface between surfaces involves contact and separation. In other words, the transmission of force between the surfaces occurs when they are in contact. For this reason, the concrete can not penetrate through the steel tube even if the concrete is subjected to the compressive force exerted by the steel tube. The top and the bottom of the column were fabricated with hinges for this analysis, and displacement of the half model was confined in the out-of-plane directional axis of the cut surface. This study does not address the issue of fracture propagation. This work is concerned with potential cracking only due to the development of stress and strain that would facilitate the fracture or other irregularity. Analyses for the validation of experimental results involved cyclic loading condition, whereas parametric analyses are used for monotonic loading condition.

3.2. Response indices

A number of different stress, strain, and combined stress/strain indices as performance indicators were computed in this study to compare the behaviors of different configurations being analyzed in this research and to assess the effect of the parameters of interest. El-Tawil *et al.* (1998; 1999; 2000) used these performance indicators in order to investigate the effect of panel zone yielding on potential fracture of welded-and-bolted steel connections and the effect of local geometric details as well as the effect of yield-to-ultimate stress ratio on the inelastic behavior of pre-Northridge connections. Some of the stress and strain indices employed in this study are described as it follows.

3.2.1. PEEQ Index

This index is defined as the plastic equivalent strain divided by the yield strain. It is a measure of local strain demand. The plastic equivalent strain (PEEQ) is defined as:

$$PEEQ = \frac{\sqrt{\frac{2}{3}\varepsilon_{ij}\varepsilon_{ij}}}{\varepsilon_y} \quad (1)$$

Where, ε_{ij} plastic strain components in directions i and j and i, j = global directions, i = 1, 2, 3, and j = 1, 2, 3; ε_y yield strain of steel.

This index is a measure of local inelastic demand and is also useful in comparing different configurations of analysis object.

3.2.2. Mises Index

This index is defined as the Von Mises stress divided by yield stress. The Mises stress, $\bar{\sigma}$, is defined as follows:

$$\bar{\sigma} = \sqrt{\frac{2}{3}S_{ij}S_{ij}} \quad (2)$$

Where $S_{ij} = \sigma^{ij} + \sigma_m\delta_{ij}$, deviatoric stress components; σ_{ij} = Cauchy stress components; $\sigma_m = -\frac{1}{3}trace(\sigma_{ij})$ mean

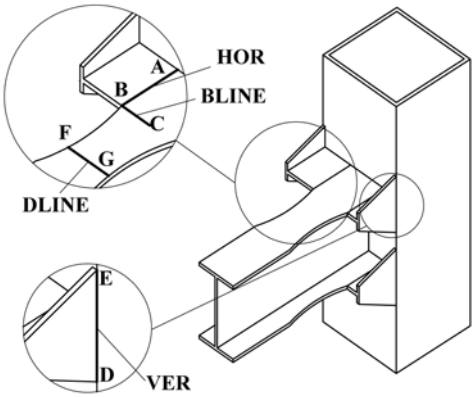

Figure 8. Locations at which stresses and strains are extracted.

hydrostatic stress; d_{ij} = Kronecker delta.

Because cracks are not explicitly modeled in the finite-element model, principal stress is used as an indicator of the potential for brittle fracture. If a crack or some other flaw exists, high principal stresses will create large stress intensity factors at the crack tips, which increase potential brittle fracture. Brittle fracture occurs abruptly and is not accompanied by significant global plastic deformation.

3.2.3. Rupture Index

The rupture index (RI) is defined as the ratio of plastic equivalent strain index to ductile fracture strain.

$$RI = \frac{PEEQ}{exp\left(-1.5\frac{\sigma_m}{\bar{\sigma}}\right)} \tag{3}$$

The ratio of hydrostatic stress to von Mises stress ($\sigma_m/\bar{\sigma}$) that appears in the denominator of Eq (3) is called triaxiality ratio. High triaxiality can cause significantly reduced rupture strain of a material, thereby limiting its ductility (El-Tawil *et al.*, 1998; 1999; 2000). Thus, locations of a connection with higher value of RI will have a greater potential for fracture.

The locations determined to have the highest fracture potential for different configurations of the analysis objects are H-HAZ (A-B), BLINE (B-C), V-HAZ (D-E), and DLINE (F-G), as shown in Fig. 8. The welded line between horizontal element and beam flange, denoted by "H-HAZ", is of interest because of the potential for weld crack in the heat affected zone (cf. the photo of Fig. 12(g)). The line at the tip of the horizontal element, denoted by "BLINE", is important because many of the observed cracks initiated from this region (Shin *et al.*, 2004; 2008). The line at the center of the RBS cutout denoted by "DLINE" was selected for the observation of detailed behavior of the reduced beam section. Finally, the welded line between vertical element and column web, denoted by "V-HAZ", is important for the analysis because a number of fractures were observed in the vertical element HAZ region (cf. the photo of Fig. 12(b) & (d)). Comparisons of these locations for the failure mode are made in this study with the story drift of 0.03 rad of plastic rotation.

3.3. FEM verification

The FEM was validated for this study by comparing measured cyclic response of the specimen TSH100 (Shin *et al.*, 2008) with predicted response. Fig. 9 shows the comparisons of the moment-total rotation hysteresis loop as well as moment-plastic rotation. The measured stress-strain properties of the materials reported by Shin *et al.* (2008) are used for this analysis. The analytical hysteresis loop corresponded well with the test data. In addition to the hysteretic behavior shown in Fig. 9, elastic stiffness, yield moment, and plastic rotation computed by the analysis program were also found to correspond well with the measured responses, as summarized in Table 1. In addition, Fig. 5 shows the comparison of the longitudinal strains in the beam flange from the experiment and analysis. The predicted strains on the beam flange from the FEM also show good agreement with test data, displaying consistent trends with the experimental data.

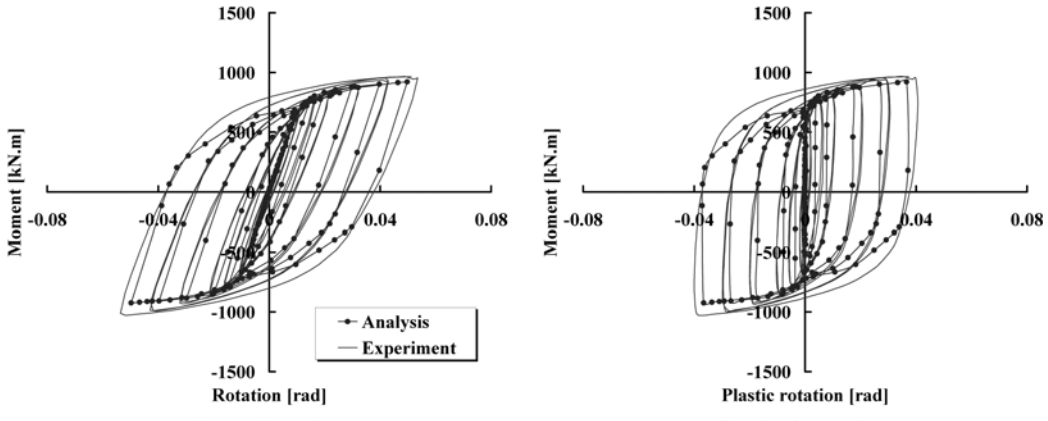

(a) Total rotation (b) Plastic rotation

Figure 9. Comparison between experimental and analytical hysteretic loops (TSH100).

Table 1. Comparison between analytical and experimental results

Specimen	Initial stiffness (kN · m/rad)			Yield moment (kN · m)		
	${}_eK_i$	${}_aK_i$	${}_eK_i/{}_aK_i$	${}_eM_y$	${}_aM_y$	${}_eM_y/{}_aM_y$
TS100	6200	6500	0.95	710	707	1.00
TS120	7300	7000	1.04	739	752	0.98
TS140	7300	7400	0.99	784	775	1.01
TSD100	6500	6200	1.05	768	609	1.26
TSD120	6800	6600	1.03	699	663	1.05
TSH100	6800	6700	1.01	662	680	0.97
TSH120	7000	6700	1.04	737	751	0.98

3.4. Analytical results

Fig. 10 shows contour plots of plastic equivalent strain (PEEQ) and photos after the experiment (based on the previous research (Shin *et al*., 2008)) at 0.03 rad of connection plastic rotation (CPR). Concentration of strain occurred at the horizontal element tip for the specimens of TS100 and TS120 (Fig. 10(a)-(b)), reduced flange section of the specimens TSD100 and TSD120 (Fig. 10(d)-(e)), and near the horizontal element hole for the specimens of TSH100 and TSH120 (Fig. 10(f)-(g)). These strain concentrations of the analytical results exhibited reasonably good correlation with the failure modes of the experimental result (Shin *et al*., 2008). However, unlike the analytical results, specimens TS120 and TSD100 failed by premature facture at the vertical element welds (Fig. 10(b) & 10(d)). For the case of TS100, it was well predicted that strain would concentrate on the horizontal element before leading to failure, and tests confirmed these results (Fig.10 (a)). As for TS140, the plastic strain on its flange was extremely smaller than that of TS100. Nevertheless, the plastic strain concentrated at the vertical element due to the effect of heat-affected zone. In addition, the strength ratio of 1.0 may not be able to ensure an adequate margin of safety to transfer the force sufficiently from vertical element to column wall. However, a considerable level of plastic strain also occurred in the region near RBS for specimens TSD100 and TSD120. Especially, most plastic strain of TSD120 occurred in the region near RBS. Fig 10(e) shows a good correspondence between PEEQ and failure mode. The aforementioned performance indices were used to compare the connection configurations at different locations for more detailed investigation of analytical results.

Figure 11(a) shows PEEQ index of the vertical element V-HAZ plotted at 0.03 rad CPR. This line passes through the welded zone (V-HAZ in Fig. 8). As indicated by the PEEQ index, if the strength ratio increases while plasticization is in progress, the plastic strain of the vertical element also increases. The maximum PEEQ indices of test specimens TS120 and TS140 were 1.83 and 2.51 times, respectively, higher than that of test specimen TS100. Even within the TSD series, the maximum PEEQ index of test specimen TSD120 was 2.26 times higher than that of test specimen TSD100. On the other hand, the maximum PEEQ index of test specimen TSH120 was 2.11 times higher than that of test specimen TSH 100. This is due to the fact that as the strength ratio of the horizontal element increases and the ultimate strength of the connection also increases subsequently, greater nonlinear strain takes place on the vertical element. What is critical in this case is that a brittle fracture of the welded part or serious strain of the vertical element might occur if the plastic strain is concentrated on the vertical element, as shown in Fig. 10(b). When the comparison is made by the experimental specimen series, the PEEQ index of TSD series was significantly less than that of TS or TSH series. This is because the plastic strain is concentrated on the reduced flange of the TSD series. Even TSH series exhibited the same phenomenon when the PEEQ index of the vertical element decreased due to an increase of the plastic strain near the horizontal element hole. The maximum PEEQ index of the test specimen TSH100 was approximately 1.85 times higher than that of test specimen TSD100 and approximately 1.18 times higher than that of test specimen TS100.

Figure 11(b) shows PEEQ index of the horizontal element when the CPR is 0.03 rad. The horizontal element maintained almost constant strain value for up to approximately 2/3 of the length of the horizontal element from the column flange. However, the value increased sharply near the end of horizontal element where the end of the horizontal element met with the beam flange. The PEEQ index of the horizontal element end decreased for all experimental specimen series as the strength ratio of the horizontal element increased.

Figure 11(c) shows the PEEQ index of the beam flange BLINE plotted at CPR of 0.03. It can be seen clearly from the figure that PEEQ was the greatest at the tip of the horizontal element where the end of the horizontal element met with the beam flange and that the specimen TS100 had the largest effective plastic strain. For example, the maximum PEEQ index for TS100 was 2.57 times and 4.57 times greater than that of TS120 and TS140, respectively. The maximum PEEQ index for TSD100 was 2.38 times greater than that of TSD120. Furthermore, the maximum PPEQ index for TSH100 was 1.15 times greater than that of TSH120. This result attests for the

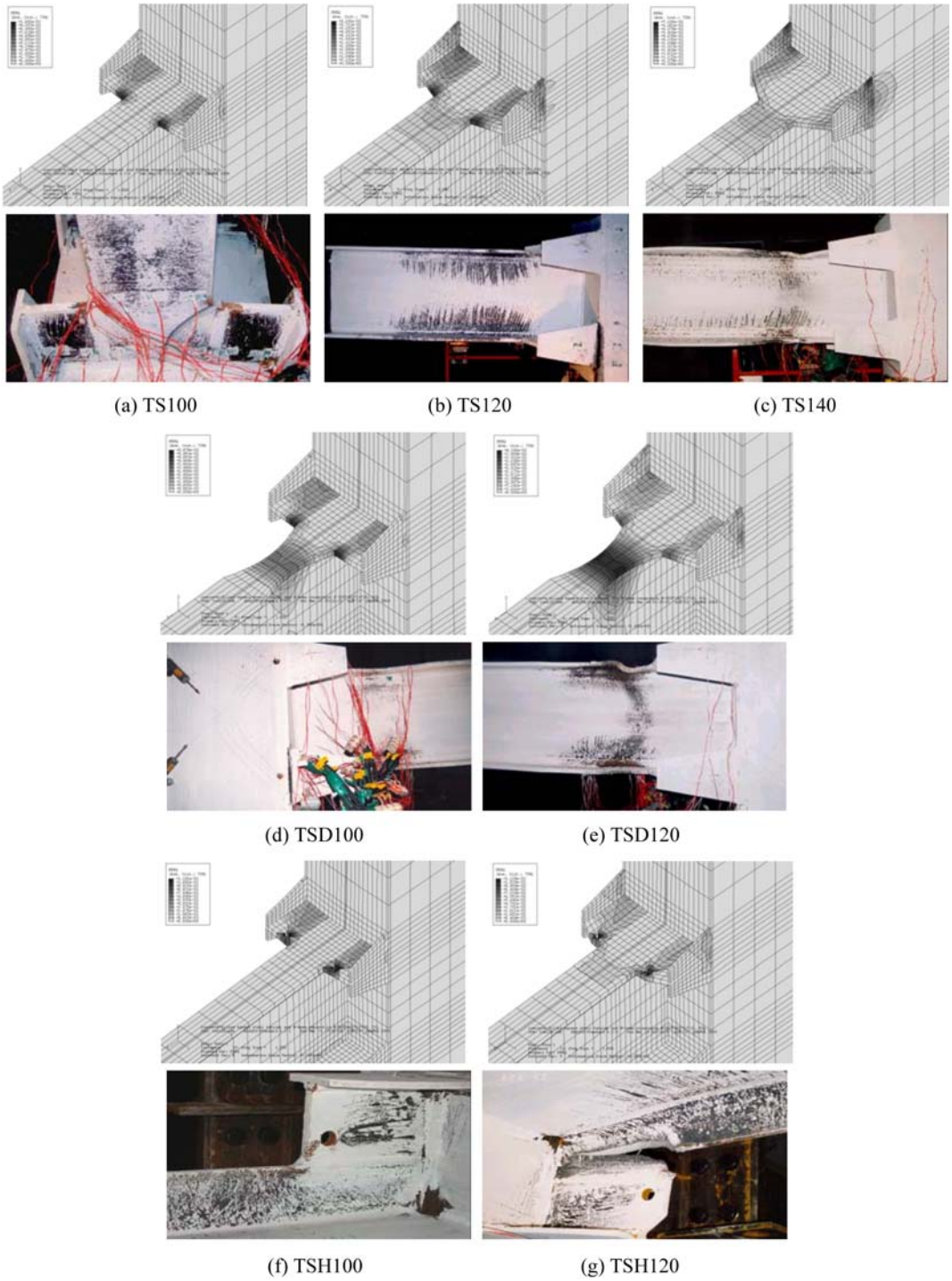

Figure 10. Contour plots of PEEQ at CPR = 0.03 and photos after test.

fact that the strain concentration was reduced as the strength ratio of the horizontal element became larger. In comparison with the differences in the maximum PEEQ index within other specimen series, the difference between TSH100 and TSH120 was relatively small, with a difference in the maximum PEEQ index of 15%. The maximum PEEQ index was 45, 23, and 29 for TS100, TSD100, and TSH100, respectively. Additionally, the maximum PEEQ index was 25, 10, and 21 for TS120, TSD120, and TSH120, respectively. This result indicates that TSD series was more effective in reducing the strain level at the connection than TSH series. There was a little effect of the strength ratio of horizontal element as for the case of TSH specimen series.

Shown in Table 2 is a summary of stress and strain indices at the tip of the horizontal element. It shows that TSD series is clearly better than TS series or TSH series from the ductile fracture point of view. This fact is well

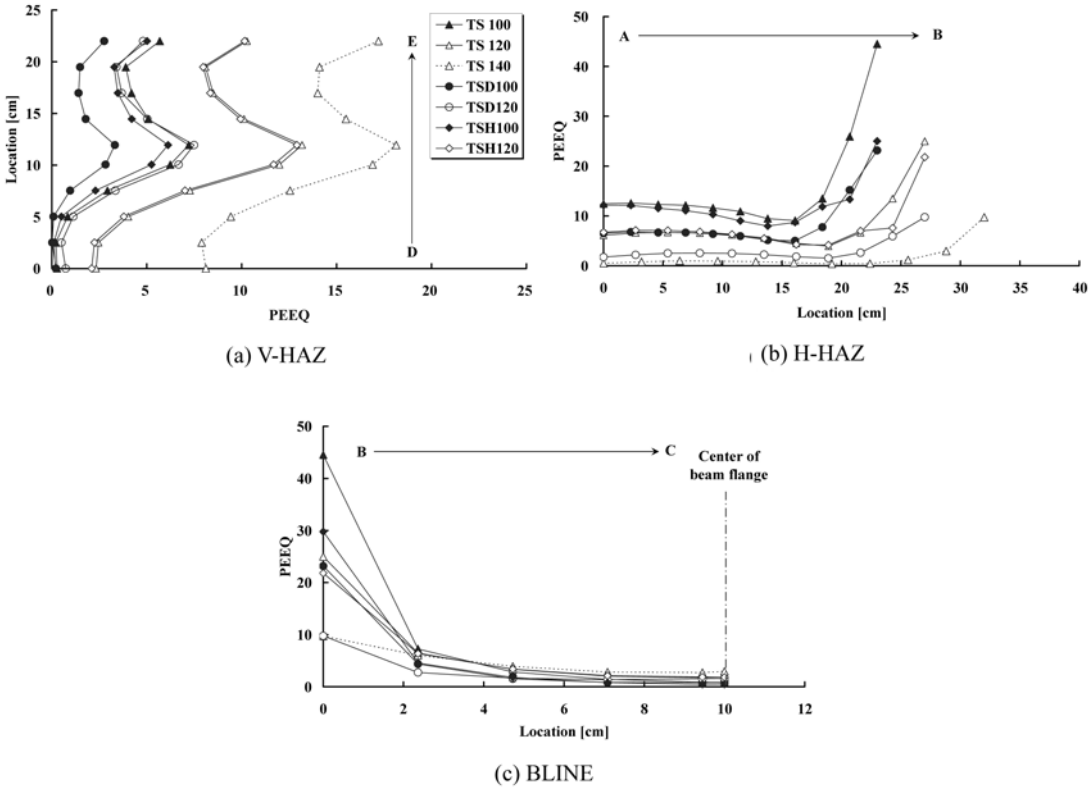

(a) V-HAZ (b) H-HAZ

(c) BLINE

Figure 11. Distribution of PEEQ indices at CPR = 0.03.

Table 2. Summary of performance indices at the tip of horizontal elements

Stress and strain indices	TS100	TS120	TS140	TSD100	TSD120	TSH100	TSH120
Mises index	1.42	1.25	1.12	1.26	1.11	1.25	1.18
PEEQ index	45	25	10	23	10	29	21
Triaxiality ratio	0.50	0.49	0.51	0.38	0.36	0.52	0.52
Rupture index	94	52	20	41	17	65	47

reflected in the rupture index, which was measured 94, 41, and 65 for TS100, TSD100, and TSH100, respectively. In addition, the rupture index was 52, 17, and 47 for TS120, TSD120, and TSH120, respectively. Furthermore, the Mises index of TSD120 was about 89 % of TS120 and about 94% of TSH120. It confirmed that by increasing the strength ratio of the horizontal element and by using a RBS cutout detail, plasticization was evenly distributed over the entire section of the flange. It is therefore important to use a RBS cutout to minimize the potential for the initiation of ductile cracking at the tip of the horizontal element.

Fig. 12(a) and 12(b) show Mises index and PEEQ index on BLINE and DLINE, respectively, of the TSD series. The maximum value of BLINE was larger than that of DLINE for the specimen TSD100, while the maximum value of BLINE crossed at a level less than the maximum value of the DLINE for the specimen TSD120. The same results were also exhibited for the case of PEEQ index. It confirmed that the horizontal element, which terminates perpendicular to the flange, manifested performance inferior to the tapered horizontal element from the ductile fracture point of view.

4. Parametric Study

Based on the analytical results of this study carried on the previous test program, it was found that a tapered horizontal element, hole drilled in the horizontal element, and RBS cutout played a significant role in reducing the plastic strain demand at the critical point of connection. Nevertheless, the effects on the local behavior of these details were not yet fully uncovered. A parametric study was, therefore, conducted to investigate the effect of local geometric details. A nonlinear analysis was carried out using the length of the vertical element and the horizontal element as well as size of the hole in the TSH series as the parameters. In addition, it was necessary to propose a connection detail capable of improving the deformation capacity and reducing the stress and strain concentration at the connection.

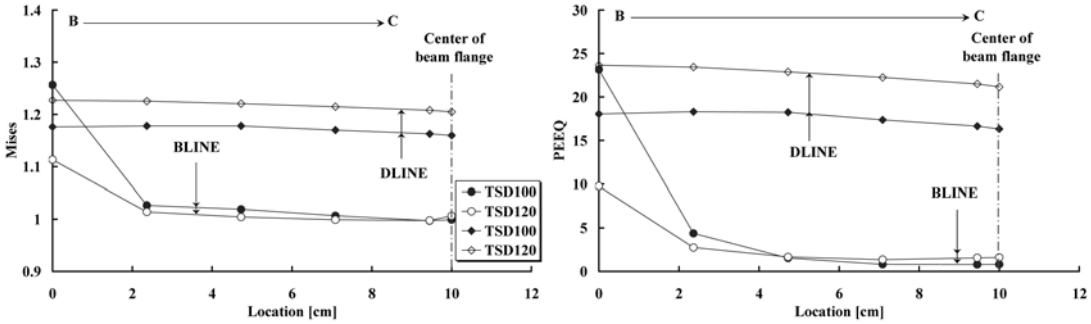

Figure 12. Mises and PEEQ indices of BLINE and DLINE.

4.1. Analytical configurations

Since the results of the analysis and experiments carried out as above indicated that the strength ratio of the vertical element of 100% was not adequate, models with the strength ratio of the vertical element increased to 120% were used as the basis. The strength ratio of 120% was adopted based on the previous research (Shin *et al*., 2008). In the previous research, it was tentatively suggested that the strain hardening factor of 1.2 be adopted as the strength ratio between vertical and horizontal element in order to develop good ductility for T-stiffener connections. Furthermore, several models with various diameter of the holes as parameters (30, 36, and 50 mm) were presented in order to investigate the effects of holes made on the TSH specimen series. Table 3 shows the list of analytic models with types of connections and strength ratio of the horizontal and vertical elements. A total of eleven analytical models are designed, which are largely classified into three series (TS series, TSD series, and TSH series). Fig. 13 shows the connection details of the TSH series of the parameter analysis models.

4.2. Parametric study results and discussions

4.2.1. TS series

The strength ratio of the vertical element was increased to 120%, and then a comparison is made with the horizontal element with the strength ratio of 120, 130, and 140%, designated as TS120V, TS130V, and TS140V, respectively. Fig. 14 shows the results of the nonlinear analysis conducted on the analytic model of the TS series, and the results of comparing PEEQ indices of H-HAZ, V-HAZ, and BLINE. TS100 is also presented as the base-line specimen in all graphs. Fig. 14(a) indicates that the maximum PEEQ index of H-HAZ is about 45 for the case of TS100 where the strength ratio of the vertical and horizontal elements was 100% but dropped to below 30 for TS120 and TS20V specimens. The PEEQ index of TS130V decreased to below 20, and that of TS140V decreased slightly. The level of decrease of TS140V was not so significant compared to TS130V. As shown in Fig. 14(b), TS140 experienced the largest strain level for V-HAZ because the strength ratio of its vertical element was 100% and plastic strain of V-HAZ increased. The PEEQ index of the TS series with the strength ratio of the vertical element increased to 120% was extremely smaller than that of 100% strength ratio. This observation suggests that, if the strength ratio of the vertical element becomes 120%, strain concentration of V-HAZ would be prevented even though the strength ratio of horizontal element increases. Fig. 14(c) plots the distribution of

Table 3. List of analytic models for parameter analysis

Specimen		Vertical element		Horizontal element		Taper	RBS cutout	Hole Size
		V/B[a] (%)	Height (mm)	H/B[b] (%)	Length (mm)			
TS series	TS120V	120	264	100	230	Yes	-	-
	TS130V	120	264	120	270	Yes	-	-
	TS140V	120	264	130	320	Yes	-	-
TSD series	TSD120V	120	264	120	270	Yes	Yes	-
	TSD130V	120	264	130	300	Yes	Yes	-
TSH series	TSH100A	100	220	100	230	-	-	$\phi = 30$
	TSH100B	100	220	100	230	-	-	$\phi = 36$
	TSH100C	100	220	100	230	-	-	$\phi = 50$
	TSH130AV	120	264	130	300	-	-	$\phi = 36$
	TSH130BV	120	264	130	300	-	-	$\phi = 36$
	TSH130CV	120	264	130	300	-	-	$\phi = 50$

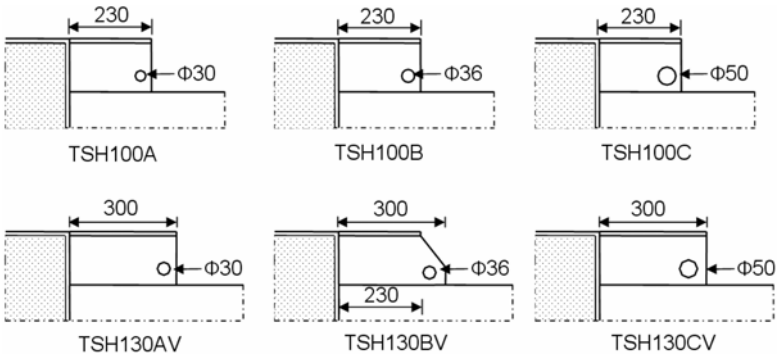

Figure 13. Details of TSH series.

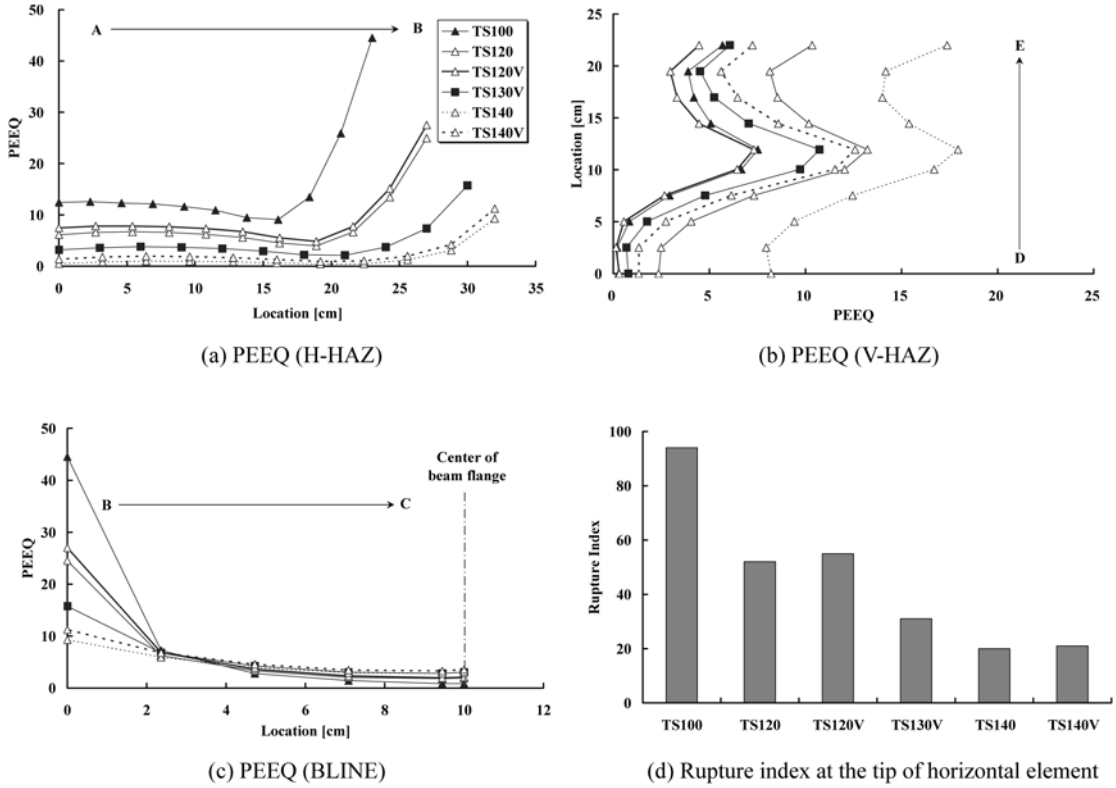

Figure 14. Performance indices (TS series).

PEEQ index of BLINE. TS130V and TS140V presented relatively low PEEQ indices. Fig. 14(d) shows rupture index of TS series at the tip of horizontal element. These plots revealed that the gradual change in tapered shape from beam flange to horizontal element resulted in a considerable reduction of the concentration of strain at BLINE. Most of all, it is worth noting that the plastic strain level of BLINE can remarkably be reduced for the case of TS series if the strength ratio of horizontal element exceeds 130%.

4.2.2. TSD series

Just like the case of TS series, the strength ratio of the vertical element of TSD series was increased to 120%, and a nonlinear analysis was carried out using models with horizontal element strength ratios of 120% and 130%, designated as TSD120V and TSD130V, respectively. Fig. 15(a) demonstrates that the PEEQ indices of the horizontal element of the TSD 120V and TSD130V are extremely smaller than that of TS100. As it can be seen in Fig. 15(b), it is deemed that, if the strength ratio of the vertical element is increased to 120%, the strain concentration of the vertical element can be reduced similar to the results of TS series even with the increase in the strength ratio of the horizontal element. Even if the strength ratio of the vertical element of the TSD series with RBS was increased to 100%, the PEEQ index of the vertical element, influenced by the increase in the strength ratio of the horizontal element, did not exceed 8. For this reason, it is construed that the ductile behavior of such a connection can be induced even if the strength ratio of the vertical element is set at 100%. It is, however,

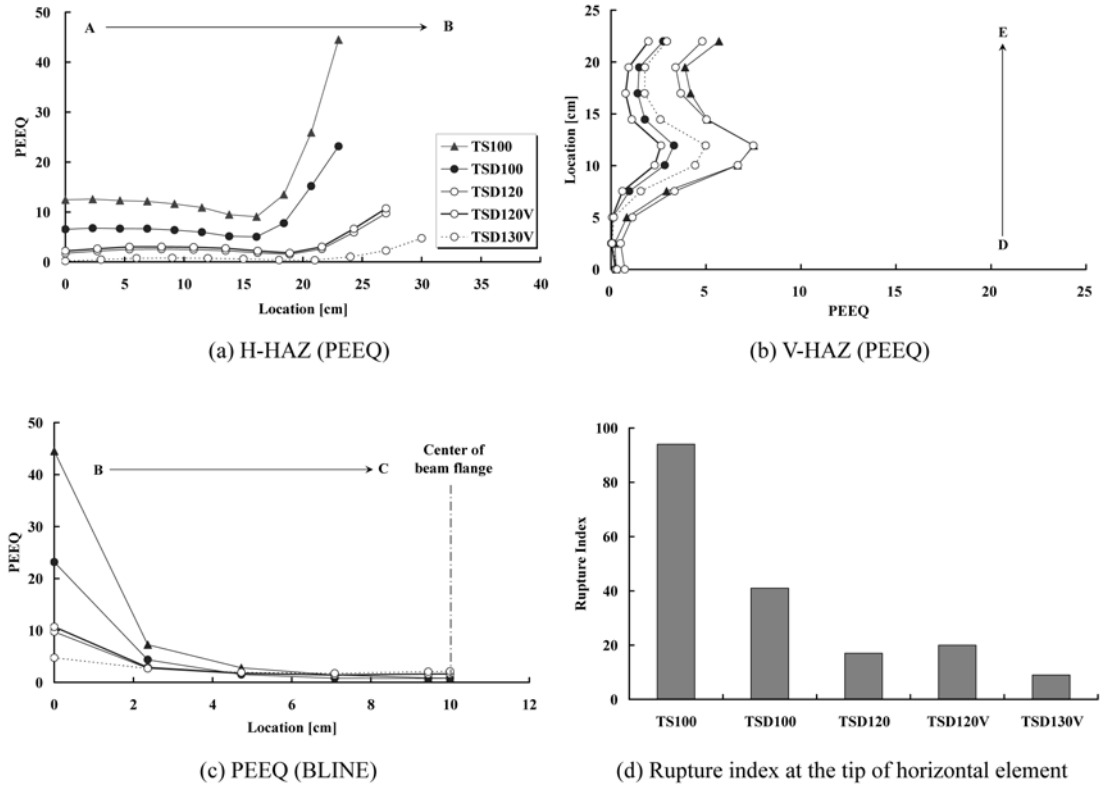

Figure 15. Distribution of PEEQ indices (TSD series).

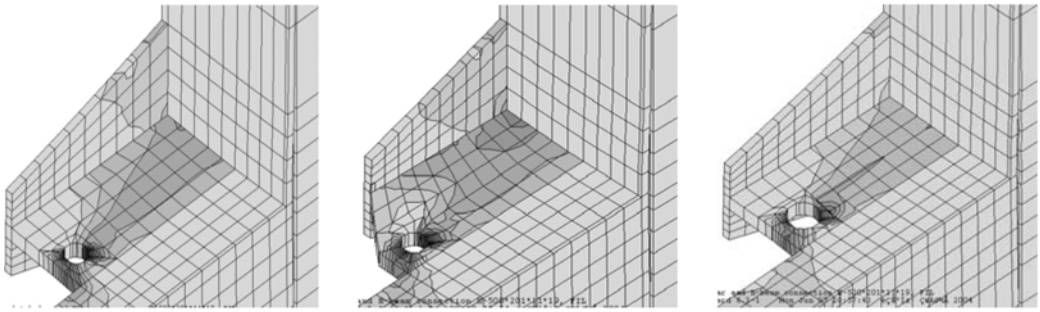

Figure 16. Contour plots of PEEQ at CPR = 0.03.

necessary to consider that strength ratio of over 120% would be appropriate for T-stiffener connection, focusing on the strain-hardening effect of material. This fact was confirmed through the previous test (Fig. 10(b) and Fig. 10(d)). Fig. 15(c) and Fig. 15(d) also revealed that the plastic strain level of BLINE for TSD series can be significantly reduced and can be made smooth if the strength ratio of horizontal element exceeds 120%.

4.2.3. TSH series

Fig. 16 shows contour plots of TSH130AV, TSH130BV, and TSH130CV. It illustrates the concentration of plastic strain in the vicinity of the hole. Fig. 17 shows the PEEQ index and rupture index of H-HAZ, V-HAZ, and BLINE when the CPR of the TSH series is 0.03 rad. Fig. 17(a) reveals that, as the strength ratio of horizontal element increases or as the size of the hole drilled into the horizontal element increases, the PEEQ index of the horizontal element end connected to the beam flange decreases slightly. As shown in Fig. 17(c), regarding TSH130 series with 130% strength ratio of its horizontal element, the PEEQ index was reduced at point around B with the increase in the size of the hole. The index level, however, was larger than that of TS130V, which had no hole, indicating that the effects of the hole were inconsistent. This result was also confirmed from rupture index point of view. Fig. 17(d) also reveals that the effect of the drilled hole in horizontal element was insignificant, although the strain level at the tip of horizontal element decreased slightly due to the drilled horizontal element.

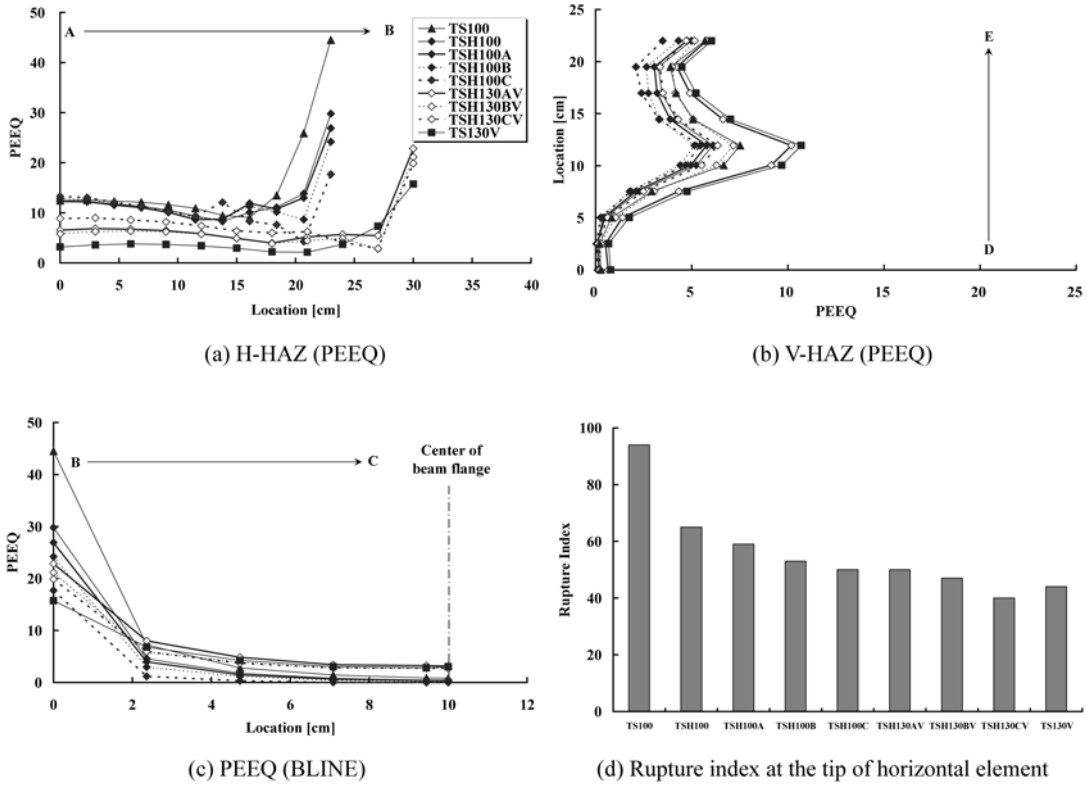

Figure 17. Distribution of PEEQ indices (TSH series).

4.3. Design considerations

The analysis was carried out using the strength ratio of the vertical and horizontal elements and the size of the hole in the horizontal elements as parameters. The results for TS series indicates that, when the strength ratio of the vertical element and horizontal element is set at 120% and 130%, respectively, the stress concentration of the test specimen is reduced in the region expected of the concentration build-up, indicating that it is a model effective in inducing a ductile failure. It is also found that TSD series with the strength ratio exceeding 120% exhibit PEEQ index and rupture index significantly smaller than that of other details. This in turn indicates that sufficient deformation capacity can be demonstrated in the region near RBS cutout, inducing a beam collapse mechanism by pushing the plastic hinge at the end of T-stiffener. Results for the TSH series point out that, when a connection with drilled holes in the horizontal element is used, stress concentration is reduced, thereby promoting the efficiency of the members. However, there are no consistent results of the current analysis from which to derive conclusions and provide guidelines for actual design as of yet within the scope of this study. Nevertheless, several recommendations based on the results of this research are presented in the following conclusions.

5. Conclusions

The influence of local geometric details such as a horizontal element, a vertical element, and a hole in the horizontal element on the stress-transfer mechanism of CFT column-to-beam moment connections has been investigated using a 3D nonlinear finite element model. Based on the parametric studies of full-scaled subassemblies, the key points of the derived conclusions are noted below.

Fractures initiating at the tip of the horizontal elements were observed in numerous inelastic cyclic connection tests with T-stiffener details in the past. An effort was made to investigate the influence of horizontal element geometry and its strength ratio to beam on the potential for the initiation of a ductile fracture near the T-stiffener end. The results point to the importance of properly selecting a horizontal element configuration. The gradual change in the tapered shape from beam flange to horizontal element resulted in a considerable reduction of the strain concentration near the connection. As mentioned earlier, when the ratio of the horizontal element strength to the beam flange strength (*H/B*) increases, its inner length only is increased while the outer length of the horizontal element is unchanged, as it transits from a rectangular section to a tapered section. For TS series, a horizontal element, of which the strength ratio to beam

exceeds 130%, is recommended for seismic resistant design. In addition, the analyses of this study suggest that it is important to use a vertical element, of which the strength ratio to beam exceeds 120%, to minimize the potential for a brittle fracture at the heat-affected welded zone. Based on the strain-hardening effect of steel material, strength ratio of 120% for vertical element is recommended.

Regarding the experiments with TSD specimen series, T-stiffener is used to supplement the reduced beam section to further limit the stress in beam flange. RBS cutout was found to have a significant effect on the fracture potential of the beam flange near the horizontal element end. Based on the analysis results, conditions effective for plastic strain and rupture index were significantly reduced at beam flange near the horizontal element end. Hence, strength ratio of 120% for TSD series is recommended. TSD series with RBS cutout results in a significant reduction in the PEEQ index and rupture index in comparison with TS series. Thus, the strength ratio of TSD series slightly lower than that of TS series as much as 10% difference should be adopted.

The results for TSH specimen series reveals that, as the strength ratio of the horizontal element increases or as the size of the hole drilled into the horizontal element increases, the PEEQ index of the horizontal element end connected to the beam flange decreases slightly. Of a particular notice was that there was inconspicuous difference whether drilled hole exist or not as for the horizontal element. Moreover, there were no consistent results of the current analysis from which to derive conclusions and provide guidelines for actual design as of yet. More experiments and analytical study are needed to develop the optimum connection details with respect to the size and location of the holes drilled into the horizontal element.

Some of the above findings and recommendations have been verified and supported by full-scale inelastic cyclic testing of CFT column-to-beam subassemblies. Further research is necessary to investigate the behavior of connections having different details and member section sizes so that more generalized recommendations can be offered.

References

ABAQUS (2002). *Standard user's manual*. Version 3, Habbit, Karlsson & Sorensen Inc.

Azizinamini, A.A. (2005). "Design of through beam connection detail for connecting steel beams to circular concrete-filled steel tube columns." *International Journal of Steel Structures*, KSSC, 5(4), pp.349-356.

Azizinamini, A.A. and Schneider, S.P. (2004). "Moment connections to circular concrete-filled steel tube columns." *Journal of Structural Engineering*, ASCE, 130(2), pp.213-222.

Cheng. C-T. and Chung, L-L. (2003). "Seismic performance of steel beams to concrete-filled steel tubular column connections." *Journal of Constructional Steel Research*, 59(3), pp. 405-426.

El-Tawil, S., Mikesell, T., Vidarsson, E., and Kunnath, S.K. (1998). "Strength and ductility of FR welded-bolted connections." Rep. No. SAC/BD-98/01, ATC, Redwood City.

El-Tawil, S., Vidarsson, E., Mikesell, T., and Kunnath SK. (1999). "Inelastic behavior and design of steel panel zones." *Journal of Structural Engineering*, ASCE, 125(2), pp.183-193.

El-Tawil, S., Mikesell, T., and Kunnath, S.K. (2000). "Effect of local details and yield ratio on behavior of FR steel connections." *Journal of Structural Engineering*, 126(1), pp.79-87.

Fujimoto, T., Nishiyama, I., and Mukai, A. (1997). "Test results of CFT beam-to-column connection." US-Japan cooperative earthquake research program: Composite and hybrid structures. *4th JTCC*.

Fukumoto, T. and Morita, K. (2000). "Elasto plastic behavior of steel beam to square concrete filled steel tube(CFT) column connections." In: Mahin SA, Xiao Y, editors. Composite and hybrid structures: *Proc., 6th ASCCS int. conf. steel-concrete composite structures*. Pp.565-572.

Kang, C.H., Shin, K.J., and Oh, Y.S., and Moon, T.S. (2001). "Hysteresis behavior of CFT column to H-beam connections with external stiffeners and penetrated elements." *Engineering Structures*, 23(9), pp.1194-1201.

Kimura, K., Chung, J., Matsui, C., and Choi, S. (2005). "Structural characteristics of H-shaped beam-to-square tube column connection with vertical stiffeners." *International Journal of Steel Structures*, KSSC, 5(2), pp.109-117.

Matsuda, H., Tanaka, A., Ishimura, R., Hirai, K., and Sasaji, S. (2000). "Experimental study on the statistical characteristics of perimeter beam-to-SHS column connections using vertical stiffener plates." *Journal of Structural and Construction Engineering*, AIJ, 534(8), pp.167-174

Morino, S. and Kawaguchi, J. (2005). "Research on and construction of the concrete-filled steel tube column system in Japan." *International Journal of Steel Structures*, KSSC, 5(4), pp.277-298.

Nishiyama, I., Fujimoto, T., Fukumoto, T., and Yoshioka, K. (2004). "Inelastic force-deformation response of joint shear panels in beam-column moment connections to concrete-filled tubes." *Journal of Structural Engineering*, ASCE, 130(2), pp.244-252.

Ricles, J.M., Lu, L.W., Sooi, T.K., and Vermass, G. (1996). Seismic performance of CFT column-to-WF beam moment connections. *Connections in Steel Structures: Behavior, strength & design*, Bjorhovde, R., Colson, A., and Zandonini, R., Pergamon, pp.99-114.

Ricles, J.M., Peng, S.W., and Lu, L.W. (2004). "Seismic behavior of composite concrete filled steel tube column-wide flange beam moment connections." *Journal of Structural Engineering*, ASCE, 130(2), pp.223-232.

Shanmugam, N.E. and Ting, L.C. (1995). "Welded interior box-column to I-beam connections." *Journal of Structural Engineering*, ASCE, 121(5), pp.824-830.

Shin, K.J., Oh, Y.S., and Moon, T.S. (1998). "Test of

concrete-filled box column to H-beam connections." *Proc. Of 5th Pacific structural steel conference*, Korea Society of Steel Construction, Korea, pp. 881-886.

Shin, K.J., Kim, Y.J., Oh, Y.S., and Moon, T.S. (2004). "Behavior of welded CFT column to H-beam connections with external stiffeners." *Engineering Structures*, 26(13), pp.1877-1887.

Shin, K.J., Kim, Y.J., and Oh, Y.S. (2008). "Seismic behavior of composite concrete-filled tube column-to-beam moment connections." *Journal of Constructional Steel Research*, 64(1), pp.118-127.

Wu, L-Y., Chung, L-L., Tsai, S-F., Lu, C-F., and Huang, G-L. (2007). "Seismic behavior of bidirectional bolted connections for CFT columns and H-beams." *Engineering Structures*, 29(3), pp.395-407.